Nanoscale

REVIEW

View Article Online
View Journal | View Issue

Cite this: *Nanoscale*, 2017, **9**, 994

Antibacterial mechanisms of graphene-based composite nanomaterials

Mauricio D. Rojas-Andrade,[a] Gustavo Chata,[a] Dara Rouholiman,[a] Junli Liu,[a,c] Chad Saltikov*[b] and Shaowei Chen*[a]

Received 8th November 2016,
Accepted 9th December 2016

DOI: 10.1039/c6nr08733g

www.rsc.org/nanoscale

Pathogenic bacteria are gaining resistance to conventional antibiotics at an alarming rate due to overuse and rapid transfer of resistance genes between bacterial populations. As bacterial resistance to antibiotics causes millions of fatalities worldwide, it is of urgent importance to develop a new class of antibiotic materials with both broad-spectrum bactericidal activity and suitable biocompatibility. Graphene derivatives are rapidly emerging as an extremely promising class of antimicrobial materials due to their diverse bactericidal mechanisms and relatively low cytotoxicity towards mammalian cells. By combining graphene derivatives with currently utilized antibacterial metal and metal–oxide nanostructures, composite materials with exceptional bactericidal activity can be achieved. In this review, the antibacterial activities of graphene derivatives as well as their metal and metal–oxide composite nanostructures will be presented. The synthetic methodology for these various materials will be briefly mentioned, and emphasis will be placed on the evaluation of their mechanisms of action. This information will provide a valuable insight into the current understanding of the interactions governing the microbial toxicity of graphene-based composite nanostructures.

1. Introduction

Graphene is currently the subject of intense research due to the unique optical, electronic, and mechanical properties that result from its two-dimensional sp^2-hybridized carbon structure. Recently, there has been particular interest in using graphene nanomaterials for biomedical applications, such as drug delivery, sensing, tissue regeneration, and cancer therapy.[1–7] As graphene nanostructures have been found to exhibit limited toxicity towards eukaryotic cells, the utilization of graphene derivatives for biological applications has been attracting significant attention from the scientific community.[8–12]

A particularly alarming issue in world health today is the rise and prevalence of antibiotic-resistant bacteria, which significantly increases death rates and costs of treatment. According to the World Health Organization, many countries around the world have observed last-resort antibiotics to be ineffective in over half of patients afflicted by common pathogenic bacteria such as *Escherichia coli* and *Klebsiella pneumoniae*. Even more alarming is the prevalence of antibiotic-resistant bacteria in countries with advanced medical facilities such as the United States, where, according to the CDC, over 2 million people become infected by these resistant pathogens leading to over 23 000 deaths annually. Therefore, it is imperative that as these antibiotic-resistant bacteria evolve, so must the medicines that are utilized to treat them. To this end, antibacterial nanostructures have recently gained serious consideration by the healthcare community.[13,14] The antibacterial applications of graphene-based nanomaterials are still relatively new however. In fact, although there are several excellent reviews that summarize recent progress in the studies of the antimicrobial activity of graphene nanostructures, few discuss the mechanisms of action in detail.[15–20] In order to develop next-generation antimicrobial materials, a comprehensive understanding of the mechanisms of action of graphene nanostructures as well as their metal and metal–oxide derivatives is desired.

This review will summarize recent progress towards an understanding of the cytotoxicity mechanisms of graphene-based nanostructures, with a focus on studies providing evidence for oxidative stress induction and membrane disruption.

[a]*Department of Chemistry and Biochemistry, University of California, 1156 High Street, Santa Cruz, California 95064, USA. E-mail: shaowei@ucsc.edu*
[b]*Department of Microbiology and Environmental Toxicology, University of California, 1156 High Street, Santa Cruz, California 95064, USA. E-mail: saltikov@ucsc.edu*
[c]*School of Materials Science and Engineering, Shaanxi University of Science and Technology, Xi'an, 710021, China*

2. Cytotoxicity of graphene composite nanomaterials

Study of the cytotoxicity of graphene nanomaterials is a relatively new field. Accordingly, mechanistic models have yet to

be established. Although a mechanism of action is generally provided in many studies, the experimental evidence substantiating most claims is generally limited. The most commonly proposed mechanisms of action fall under four categories: (a) oxidative stress induction,[21–23] (b) protein dysfunction,[24,25] (c) membrane damage,[23,26,27] and (d) transcriptional arrest.[28,29] Independently, these represent unique cellular toxicities with specific biomolecular targets such as iron–sulfur clusters, cysteine residues of proteins, membrane lipids, and DNA molecules. However, as biological processes are intricately linked, the exact effects of nanomaterial toxicity are difficult to isolate. Compounding the problem even further, each of these forms of toxicity can independently result in the other three, with the generation of reactive oxygen species (ROS) being the most commonly reported outcome. It is understandable then that the exact mechanism of nanomaterial cytotoxicity is obscure, resulting in largely speculative claims based on indirect evidence. An overview of the proposed mechanisms of cytotoxicity for a variety of graphene, graphene–metal, and graphene–metal oxide nanostructures is given in Table 1, which, although incomplete, is representative of the current understanding. As *in vitro* experiments such as glutathione (GSH) oxidation and ROS-generation assays are utilized to provide evidence for a specific mechanism of action, the cytotoxic effects of these nanomaterials inside bacterial cells are typically oversimplified.[30–35] In order to completely and accurately describe the mechanisms of toxicity that nanomaterials exhibit in a cellular environment, researchers at the forefront of this field will need to take a highly interdisciplinary approach utilizing both chemical and biological techniques to substantiate their claims. Below we will highlight some recent progress in this area of research.

2.1 ROS generation and cytotoxicity

The formation and cytotoxicity of ROS has been a universal theme in nanomaterial toxicity. Numerous studies on metal, metal oxide, and most interestingly, carbon-based nanomaterials have claimed the formation of ROS to be the primary mechanism of cytotoxicity.[36–42] However, substantial direct evidence demonstrating this has yet to be provided. As oxidative stress results from nearly all forms of cellular cytotoxicity, such claims leave the true underlying mechanism of action insufficiently explained.

For certain metallic ions such as Fe^{2+} and Cu^{+}, ROS can be generated directly when these ions react with H_2O_2 to form hydroxyl radicals commonly known as the Fenton reaction.[43,44] The thermodynamics of hydroxyl radical generation *via* Fenton chemistry is governed by the general redox reaction,

$$F^{n+} + H_2O_2 \rightarrow F^{(n+1)+} + OH^- + OH^\bullet \quad (1)$$

where F is the Fenton-active species. The standard potential $\left(E_1^\circ\right)$ of the reaction is defined as the sum of two half-reactions,

$$F^{(n+1)+} + e^- \rightarrow F^{n+} \quad (2)$$

$$H_2O_2 + e^- \rightarrow OH^- + OH^\bullet \quad (3)$$

where E_2° and E_3° represent the reduction potentials of eqn (2) and (3), respectively, yielding an overall expression of $E_1^\circ = E_3^\circ - E_2^\circ$ for the Fenton reaction. Since $E_3^\circ = +0.279\,V$ at pH 7.6, only species with reduction potentials less positive than +0.279 V under these conditions will yield appreciable reaction rates, as governed by the relationship between Gibbs free energy and reaction potential, $\Delta G^\circ = -nFE^\circ$.[44–46] There is evidence that graphene nanomaterials are indeed Fenton-active, as demonstrated by Zhao *et al.*[47] where the Fenton-like catalytic degradation of Orange II occurred in the presence of H_2O_2 along with graphene oxide (GO) and hydrogen-reduced graphene oxide (hrGO) nanosheets. The oxidation of Orange II was found to be much less efficient with GO than with hrGO, which the authors attributed to the increasing number of defects in the sp^2 domains produced by hydrogenation. This study suggests that there is a structural correlation between graphene nanomaterials and their redox activity, which supports the notion that direct generation of ROS *via* redox chemistry is indeed one of the mechanisms of cytotoxicity exhibited by graphene materials. Liu *et al.*[34] reached similar conclusions in their study of carbon nanomaterial reactivity towards molecular oxygen. Their results demonstrated that oxygen adsorbed on the surface of graphene primarily at defect sites, formed superoxide intermediates (*e.g.*, $O^{2\bullet-}$ and $HO_2^\bullet$) which subsequently oxidized cellular GSH and released the bound superoxide species into the environment. The proposed reaction mechanism is supported by experimental and theoretical evidence.[48,49] This provides further evidence for a semi-stepwise mechanism for ROS generation on graphene surfaces.

Other groups claim that charge transfer between graphene derivatives and redox-active species other than H_2O_2 is responsible for the generation of ROS. For instance, Li *et al.*[21] provided noteworthy evidence for this charge transfer mechanism by varying the conductive nature of the substrate onto which a graphene film was deposited and comparing the bactericidal effects. Interestingly, the antibacterial activity exhibited clear dependence on the conductivity of the graphene–metal substrates, with the inhibition of *S. aureus* and *E. coli* growth increasing in the order of graphene/SiO_2 < graphene/Ge < graphene/Cu. They proposed that respiratory chain electrons were extracted from the electron transport chain (ETC) by graphene through a charge transfer mechanism, and only when a substrate with a vacant energy state below the Fermi level of graphene was utilized, could the extracted electrons be transferred from the graphene to the circuit and cause cytotoxicity. As adenosine triphosphate (ATP), the molecule which provides the energy required for many cellular processes *via* hydrolysis of the phosphate groups, is synthesized using the energy of H^+ ions moving down the electrochemical gradient created by the redox reactions of the ETC. Extraction of these mobile electrons causes a depletion of intracellular ATP, leading to cell death. The proposed energy diagrams are shown in Fig. 1 which illustrates charge transfer from respiratory-chain redox species to graphene on these different substrates and clearly shows the barrier to charge transfer that an insulating SiO_2 substrate exhibits, which correlates well with the observed antimicrobial activity.

Table 1 Summary of antibacterial activity of graphene (G), graphene oxide (GO), and reduced graphene-oxide (rGO)

Nanomaterial	Size range	Bacterial strain	Growth media	Proposed mechanism	Ref.
G	>10 μm	*Escherichia coli* (ATCC 25922) *Staphylococcus aureus* (ATCC 25923)	Undefined	Oxidative stress *via* electron transfer from membrane to graphene	21
GO	0.010–0.753 μm^2	*Escherichia coli* (K-12)	LB	Environmental isolation by membrane-wrapping	26
GO, rGO (βME)	0.525 μm (GO) 3.40 μm (rGO)	*Pseudomonas aeruginosa*	LB	Oxidative stress *via* GSH oxidation, DNA fragmentation	37
GO, rGO (N_2H_4)	>0.60 μm	*Escherichia coli* (KACC 10005) *Salmonella*	LB	Lipid peroxidation	51
GO	0.01–0.65 μm^2	*Escherichia coli* (K12 Coli Genetic Stock Center #7740)	LB	Oxidative stress (0.01 μm^2) Cell entrapment (0.65 μm^2)	26
GO	>1.0 μm	*E. coli* (ATCC 25922); *B. subtilis* (ATCC 6051)	LB	Membrane permeabilization	27
GO	0.65 μm^2	*Escherichia coli* (MV1190) (λ-pir) (pJBA116)	LB	Physical and oxidative membrane damage	52
GO (hydrazine)	1 μm	*Escherichia coli*	LB	Physical and oxidative membrane damage	23
Ag/AgCl/rGO	3–7 μm (GO) 4–163 nm (Ag)	*E. coli* (DH5a) *Staphylococcus aureus* (ATCC26085)	LB	Oxidative stress *via* ROS generation	53
AgFe/GO	>0.15 μm (GO) 10 nm (AgFe)	*Escherichia coli* (BL21) *Staphylococcus aureus* *B. subtilis* (W800)	LB	Oxidative stress and membrane damage	33
AgPt/GO	>3 μm (GO) 10 nm (AgPt)	*Escherichia coli* (ATCC 10536)	Undefined	Membrane damage	35
PLL/Cu/rGO	>0.15 μm	*Escherichia coli* (ATCC 25922) *Staphylococcus aureus* (ATCC 6538)	LB	Disruption of ion concentration gradient	54
AgCu/GO	>1.0 μm	*Escherichia coli* (ATCC 25922) *Pseudomonas aeruginosa* (ATCC 27853) *Klebsiella pneumoniae* (ATCC 700603) *Staphylococcus aureus* (ATCC 25923) *Methicillin-resistant Staphylococcus aureus* (ATCC BAA-44)	TSB	Membrane rupture and leakage of intercellular components	55
GO-TiO_2	>0.50 μm	*Escherichia coli* (ATCC 25922)	Undefined	Physical membrane disruption and oxidative charge-transfer	56
TiO_2/GO	~4.8 μm^2	*Escherichia coli*	LB	Undefined	57
ZnO/GO	2.25 μm^2	*Escherichia coli*	LB	Membrane damage	58
ZnO/GO EPD	~50–100 nm diameter ~50 μm length	*Escherichia coli* (ATCC 25922)	Undefined	Oxidative stress *via* ROS generation	59
ZnO/Ag/SGO	100 μm^2	*Escherichia coli*	LB	Oxidative stress *via* ROS generation	60
$MnFe_2O_3$/GO	36 μm^2	*Escherichia coli*	LB	Membrane damage	61

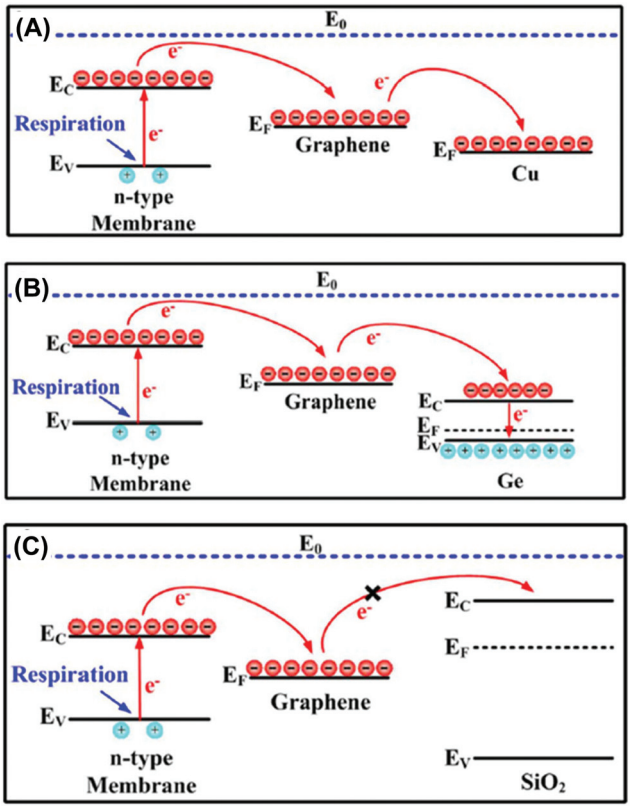

Fig. 1 Schematic energy diagrams illustrating the proposed charge transfer mechanism of (A) graphene/Cu, (B) graphene/Ge, and (C) graphene/SiO_2 substrates. Reprinted with permission from ref. 21, copyright 2014 Springer–Nature.

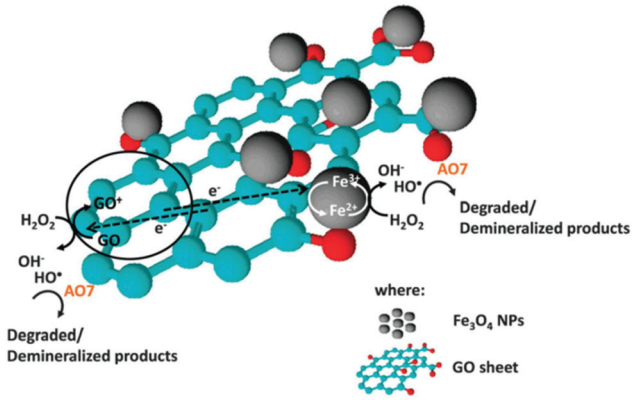

Fig. 2 Proposed mechanism of ROS generation of GO–Fe_3O_4 composite nanostructure illustrating the oxidation of sp^2 domains and subsequent transfer of electrons to local Fe_3O_4 nanoparticles. Reproduced with permission from ref. 63, copyright (2015) the Royal Society of Chemistry.

The ROS species produced from graphene and its derivatives are therefore considered to be generated through interaction with oxygen or other ETC carriers (*e.g.*, NADH, NADPH, or $FADH_2$). Table 2 lists the primary electron transporters in ETC, along with their $E°$'s at pH 7. As these biomolecules span a large range of electrochemical potentials, charge transfer reactions with graphene derivatives are likely to occur in the proximity of cellular membranes.[50]

Additionally, as graphene sheets have a large surface area, they could act as a conductive bridge over which charge transfer occurs from relatively distant redox species, further enhancing the oxidative stress potential. This has been demonstrated by Zubir *et al.*[63] through the unusually high stability of Fe atoms in GO–Fe_3O_4 composites towards Fenton reactions, which was attributed to charge transfer from the GO sheets to the oxidized Fe atoms. The authors claimed that the π electrons in the conjugated sp^2 domains facilitated electron transfer from GO to Fe_3O_4 nanoparticles *via* a Fe–O–C bond, subsequently reducing Fe^{3+} ions back to their Fe^{2+} state, thereby regenerating the Fenton catalyst (Fig. 2). Analysis of XPS spectra over the course of 7 cycles revealed a significant decrease (~19%) of the C=C peak intensity, which was accompanied by a concomitant increase in C–C and C=O intensities, suggesting oxidation of GO sheets over the cycling period. Furthermore, the Fe^{3+}/Fe^{2+} ratio increased substantially for Fe_3O_4 nanoparticles alone but exhibited a negligible change for the GO–Fe_3O_4 composite, indicating that the Fe_3O_4 nanoparticles were being stabilized in their reduced state when associated with the GO sheet. Although hydroxyl radicals formed from Fenton reactions have also been shown to oxidize graphene and other aromatic molecules, the enhanced stability of the Fe_3O_4 nanoparticles on GO, compared to Fe_3O_4

Table 2 Standard reduction potentials ($E°$) of redox systems involved in biological electron transfer at pH 7. Adapted from Roehm *et al.*[62]

Redox species	$E°$ (V)	n	Redox species	$E°$ (V)	n
Ferredoxins	−0.27–−0.5	—	UQ/UQH_2	+0.06	2
H^+/H_2	−0.42	2	$UQ^•/UQH_2$	+0.19	1
$NADP^+$/NADPH	−0.32	2	Cytochrome c_1 ($Fe^{3+/}Fe^{2+}$)	+0.22	1
$Lipoamide_{ox}/lipoamide_{red}$	−0.29	2	Cytochrome c ($Fe^{3+/}Fe^{2+}$)	+0.25	1
$FMN/FMNH_2$ [a]	−0.20	2	Riesk [2Fe–2S] ($Fe^{3+/}Fe^{2+}$)	+0.28	1
$FAD/FADH_2$ [a]	−0.20	2	Cytochrome a ($Fe^{3+/}Fe^{2+}$)	+0.29	1
Cytochrome b_L (Fe^{3+}/Fe^{2+})	−0.10	1	Cytochrome a_3 ($Fe^{3+/}Fe^{2+}$)	+0.35	1
$FAD/FADH_2$ [b]	0.0–+0.1	2	Cytochrome f ($Fe^{3+/}Fe^{2+}$)	+0.37	1
$UQ/UQH^•$	+0.03	1	O_2/H_2O	+0.82	2
Cytochrome b_H (Fe^{3+}/Fe^{2+})	+0.06	1			

[a] Free molecule. [b] Protein-bound.

nanoparticles alone, is substantial and therefore must be attributed to charge transfer from GO to Fe_3O_4 nanoparticles. These studies demonstrate that graphene materials can not only undergo redox reactions, but can also transfer charge across relatively large distances. This has significant implications for their antibacterial activity.

Metal oxides alone can also exert antibacterial activity based upon their structures. For instance, ZnO nanostructures have been known to be bactericidal, and the activity varies with the structure and the concentration of oxygen vacancies on the surface.[40,64,65] In a study by Xu *et al.*,[66] various structures of ZnO nanoparticles were synthesized, and the concentration of oxygen vacancies on the surface was controlled by hydrogen reduction, as evidenced by ESR measurements (Fig. 3A). The atomic ratios of lattice oxygens (O_L) to Zn confirmed the formation of oxygen vacancies in the ZnO nanostructures, with the highest concentration observed in the "whisker-shaped" t-ZnO sample. Interestingly, this sample showed the highest antibacterial activity, suggesting a direct correlation with the concentration of oxygen vacancies. The authors proposed that these sites could catalyze the generation of H_2O_2 as illustrated in Fig. 3B, which subsequently participated in Fenton reactions and caused cytotoxicity to bacterial cells.

Further evidence for the enhanced activity of ZnO by GO composite structures is provided by Kavitha *et al.*,[67] who synthesized a ZnO/graphene/GO composite and compared its antibacterial activity to that of ZnO alone. They observed a dramatically enhanced activity of the composite structure and attributed this to enhanced ROS generation and membrane disruption. As the GO sheets were relatively large, they likely wrapped around bacterial cells, bringing ZnO nanoparticles in close contact with the cellular surfaces and effectively increasing the local concentration of released Zn^{2+} ions in the proximity of the cell.

The photocatalytic properties of metal oxide/graphene composite materials have also been utilized for antibacterial applications, where increasing the density of heterojunctions is found to improve the antibacterial activity, due to enhanced absorption in the visible region. In an early study, sulfur-doped graphene oxide (SGO) sheets were synthesized by sulfonation reaction of GO and used as the supporting substrate on which arrays of ZnO nanorods were grown vertically and orderly by a nanocrystal-seed-directed hydrothermal method; Ag nanoparticles were then deposited onto SGO–ZnO *via* a polyol-reduction process (Fig. 4A).[60] The resulting multicomponent composite exhibited apparent absorption in the visible range, where the junction between the Ag nanoparticles and ZnO nanorods was observed to allow for resonance energy transfer from Ag to ZnO. Additionally, the photogenerated electrons of ZnO nanorods might be further transferred to the

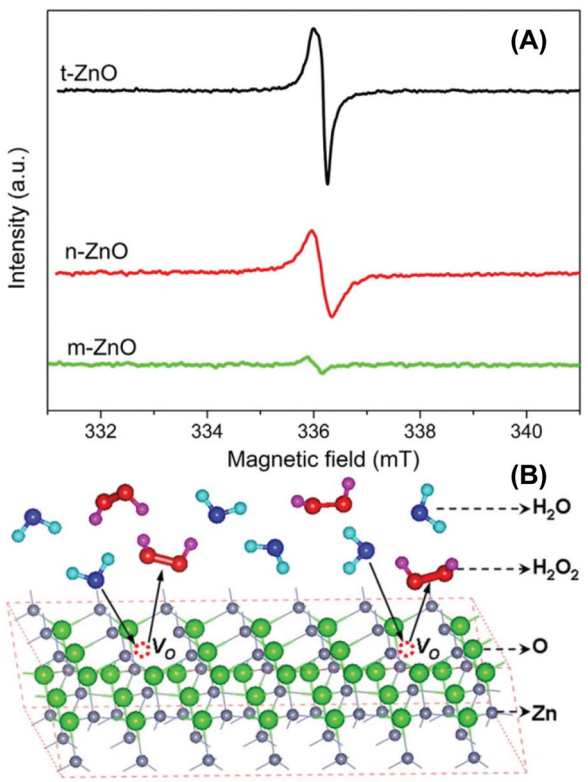

Fig. 3 (A) ESR spectra of three different types of ZnO nanostructures illustrating the extent of oxygen vacancies (V_O) within the structure, and (B) proposed mechanism of the catalytic oxidation of H_2O to H_2O_2 by oxygen vacancies in ZnO nanostructures. Reproduced with permission from ref. 66.

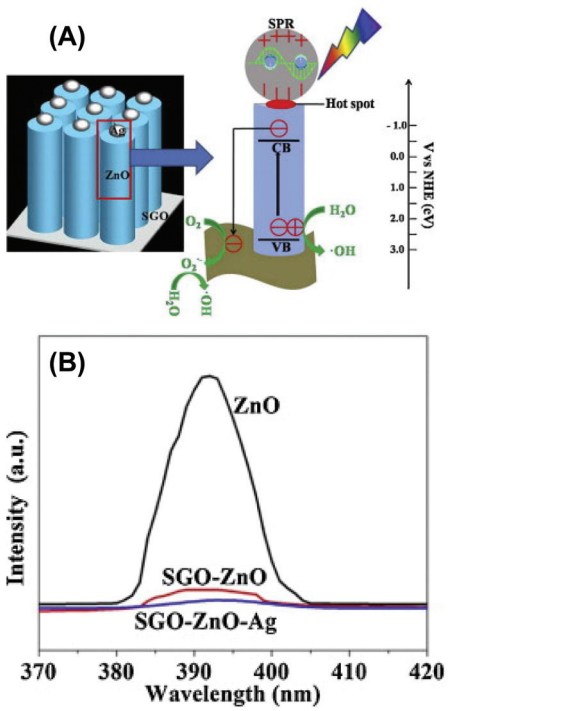

Fig. 4 (A) Schematic illustration of the surface plasmon resonance and the charge transfer route in SGO–ZnO–Ag composite. (B) PL spectra of ZnO, SGO–ZnO and SGO–ZnO–Ag composites. Reproduced with permission from ref. 60.

SGO sheets,[60] as manifested in photoluminescence studies of SGO–ZnO–Ag, SGO–ZnO, and ZnO, which suggested that electron–hole recombination was markedly impeded in the SGO–ZnO–Ag composite, since excited electrons were unable to return to the ground state following excitation (Fig. 4B). The reduced charge recombination rate was found to lead to enhanced efficiency of the formation of hydroxyl radicals and effective sterilization of *E. coli* under visible light photoirradiation.

Composites based on ZnO nanowires and graphene oxide have also been prepared by electroplating deposition (EPD), and the structure and exposed surface area have been found to afford improved interactions between the cell membrane and the metal oxide *via* membrane penetration through the creation of a "spider-like web" (Fig. 5).[59] Furthermore, photoreduction of the EPD Zn/GO composite reduced the graphene oxide sheet therein, allowing for the tuning of the graphene reduction potential to the Fermi energy level. The rate of bacteria reduction showed that EPD ZnO/GO maintained better activity than ZnO alone and ZnO/GO prepared by dropcasting (Fig. 6). The results showed that the heterojunction between the metal oxide and graphene oxide was imperative in enhancing the antibacterial activity.

In a separate study, the antibacterial activity of photocatalytically reduced TiO_2/GO hybrids was tested as a function of irradiation time with sunlight exposure.[56] Experimentally, GO platelets were first synthesized by a chemical exfoliation method and then deposited onto anatase TiO_2 thin films. The platelets thickness was about 1.7 nm, which corresponded to

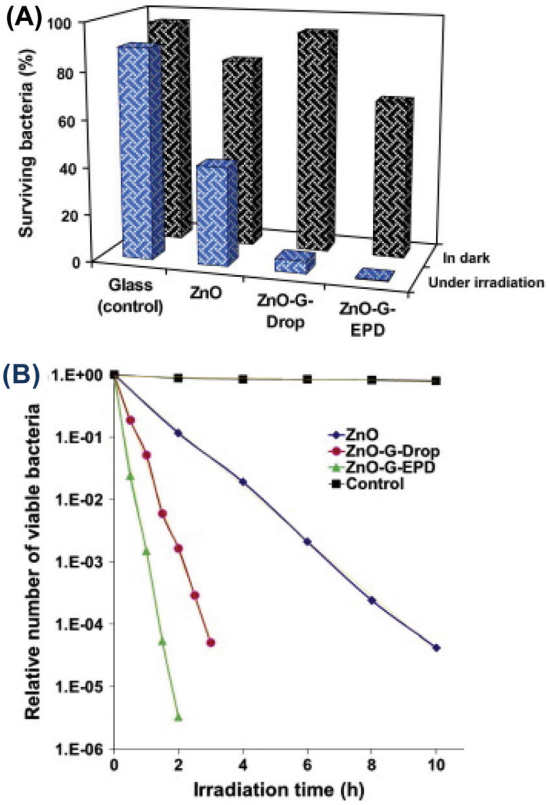

Fig. 6 (a) Percentage of surviving bacteria on ZnO NWs and GO/ZnO NW composites prepared by drop-casting and EPD methods, in dark and under visible light irradiation for 1 h, and (b) variations in the number of the viable bacteria on surface of the various samples by irradiation time. Reproduced with permission from ref. 59, Copyright (2014) Elsevier.

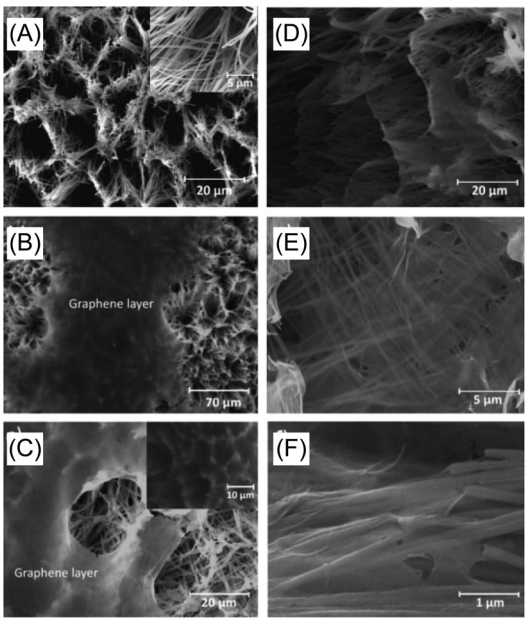

Fig. 5 SEM images of (a) ZnO NWs, (b and c) ZnO NWs partially covered with GO sheets after drop-casting deposition, and (d) GO/ZnO NW composite fabricated by EPD. (e and f) Present magnified and tilted SEM images shown in (d). Reprinted from ref. 59, Copyright (2014) Elsevier.

1–3 layers of GO. When the composites were immersed in ethanol and subjected to photoirradiation, the GO was reduced by photogenerated radicals, as manifested by XPS measurements which showed a clear reduction of the C–OH, C═O, and O═C–OH residues (Fig. 7A). The resulting rGO platelets were found to act as electron acceptors that effectively decreased the recombination rate of photogenerated electron–hole pairs, leading to enhanced phototoxicity towards *E. coli* cells in water under solar light irradiation. Fig. 7B demonstrates how reduction of graphene oxide, which serves as a substrate for TiO_2, affects the antibacterial activity of the TiO_2/GO composite upon excitation with a 110 mW cm^{-2} lamp that peaks at 275, 350, and 660 nm. Excitation by this light source produces ethoxy radicals which subsequently react with GO nanostructures, decreasing the percentage of C–OH, C═O, and O–COH. Such changes in the structure can enhance the rate of ROS generation, thereby tuning the antibacterial activity.

Furthermore, the photocatalytic activity of TiO_2/GO was found to be dependent upon the concentration of GO deposited on the metal oxides.[57] Increasing loadings of TiO_2 on GO decreased the effective band-gap of the nanocomposite causing an increase in the range of photo absorption.

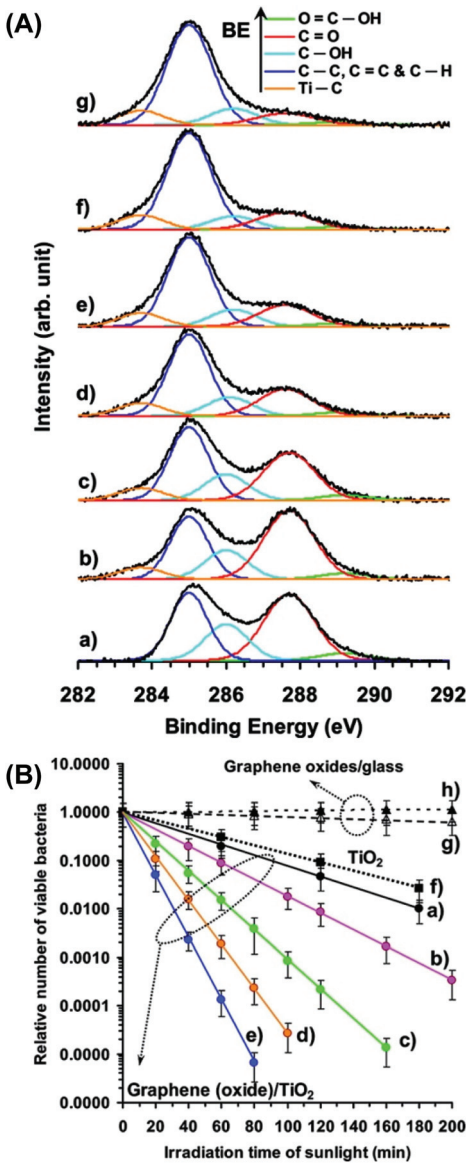

Fig. 7 (A) Peak deconvolution of the C 1s XPS core level of graphene (oxide)/TiO_2 thin films (a) as-deposited, (b) annealed at 400 °C in air, reduced by the UV–visible light-assisted photocatalytic reduction for (c) 0.5, (d) 1, (e) 2, and (f) 4 h of irradiation time in ethanol, as compared to (g) the XPS spectrum of the thin film (f) immersed in the aqueous solution containing the bacteria and under solar light irradiation for 80 min. (B) Number of bacteria cultured from the viable *E. coli* on the surface of the graphene oxide/TiO_2 thin films reduced by UV–visible light-assisted photocatalytic process for (a) 0, (b) 0.5, (c) 1, (d) 2, and (e) 4 h irradiation time, as compared to (f) number of bacteria on bare TiO_2 thin film and (g) on graphene oxide/glass film, under solar light irradiation. (h) Number of bacteria on the graphene oxides applied in part g but in the dark, as a control sample. Reproduced with permission from ref. 56. Copyright 2009 American Chemical Society.

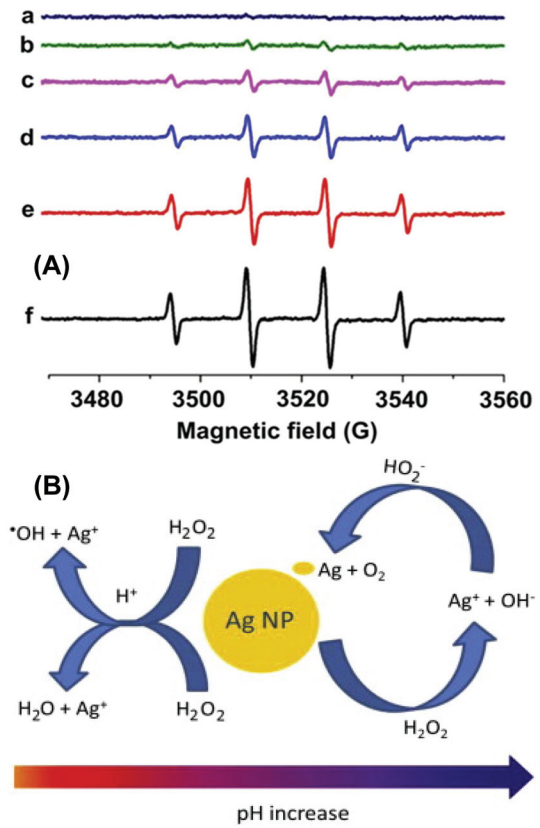

Fig. 8 (A) ESR spectra of DMPO/$OH^{\bullet}$ generated at pH 3.6 in the presence of DMPO, H_2O_2, HAc, and increasing concentrations (Aa–Af) of AgNP, (B) proposed mechanisms of ROS generation catalyzed by AgNP at different pH values. Reprinted with permission from ref. 38, Copyright (2012) Elsevier.

However, the activity of the nanocomposites was found to decrease at very high loadings of GO, and the sample at 4.2 wt % exhibited the highest activity against bacteria. The authors suggested that increasing the concentration of GO in the composite red-shifted the wavelength of maximum absorption, thereby inhibiting bacteria through enhanced ROS production. However, it remains inconclusive whether these structures become more stable/reactive and what effect this has on the observed activity.

Metal–graphene composite structures have exhibited similar enhancements of their antibacterial activity. The most commonly utilized metal for antibacterial applications is silver as it has demonstrated great promise in all forms, with nanostructured Ag materials showing the best performance. One of the most commonly claimed, and most debated mechanisms of bactericidal activity is, again, ROS production. Recent ESR evidence (Fig. 8A) by He *et al.* demonstrated catalytic generation of ROS species at varying pH by Ag nanoparticles (Fig. 8B), which supports claims made by Kim *et al.* in earlier studies.[38,68] The direct generation of ROS as well as other oxidative stress damages caused by Ag nanoparticles can therefore be enhanced with the formation of graphene composite structures, as the dispersity of the metal nanoparticles as well as the cellular contact can be improved. In fact, clear enhancement of the antimicrobial activity of Ag–GO composites, has been observed, as compared to the GO substrate or the Ag nanoparticles alone.[53,69,70]

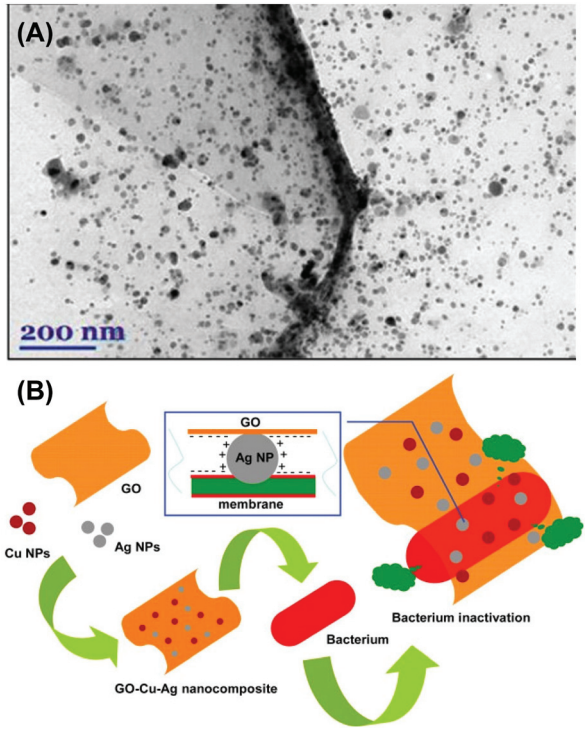

Fig. 9 (A) TEM image of AgCu/GO nanocomposite illustrating the ability of the GO substrate to prevent aggregation, and (B) illustration of the interaction and subsequent cytotoxicity of AgCu/GO composite nanostructure. Reprinted with permission from ref. 55 Copyright (2010) American Chemical Society.

Similar enhancement has been observed for GO-based composites with Cu as well as alloy (*e.g.*, FeAg, FePt, and AgCu) metal nanoparticles.[33,35,54,55] The common theme in these studies is that the cytotoxicity of metal nanoparticles is enhanced by the GO substrate, due to reduced aggregation of metal nanoparticles. This improved dispersion, as shown in Fig. 9A for AgCu alloy nanoparticles on GO, increases the active surface area, provides enhanced stability to immobilized metal nanoparticles, and localizes cytotoxic nanoparticles to bacterial membranes, as depicted in Fig. 9B. Additionally, the GO substrate affords additional membrane damaging effects, such as wrapping of bacteria and lipid extraction (*e.g.*, section 2.2), which add to the overall antibacterial performance. Understandably, there is a close relationship between the cytotoxic effects of ROS generated by nanostructured metal and metal–oxide graphene derivatives and their destructive effects on bacterial membranes. The specific mechanisms will be discussed in the following section.

2.2 Membrane disruption

Graphene and its derivatives have been observed to cause membrane damage to bacterial cells in a size and composition dependent manner.[71] Computational modelling of a single graphene sheet coming in contact with a phospholipid bilayer suggests that this interaction can induce extraction of phospholipids.[72] Due to van der Waals interactions between the

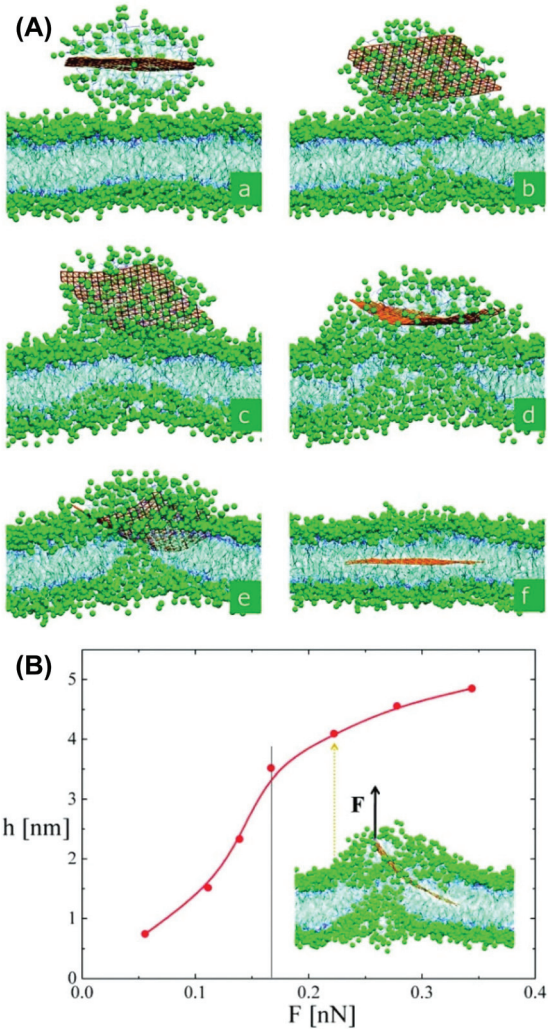

Fig. 10 Molecular dynamics simulations illustrating the insertion of a single graphene sheet into a phospholipid bilayer. (A) The interaction of the micellar graphene sheet with the phospholipid bilayer at (a) 2.9, (b) 52.4, (c) 120.0, (d) 299.2, (e) 356.4, and (f) 516.4 ns and (B) the equilibrium elevation of a single graphene sheet as a function of applied vertical force. Reproduced with permission from ref. 72. Copyright (2010) American Chemical Society.

graphene sheet and the hydrophobic moieties of this bilayer, extraction of phospholipids *via* interaction and displacement of the graphene sheet from the membrane is predicted, as shown in Fig. 10A. The force required to pull an internalized graphene sheet completely out of this model phospholipid bilayer was calculated to be 0.35 nN, yielding an extraction energy of 41.7 kcal mol^{-1}. Notably, at an elevation of around 3.5 nm above the model bacterial membrane, calculations predict membrane rupture (Fig. 10B), which has dramatic implications for the bactericidal activity of graphene sheets. These calculations provide first-principles evidence indicating that graphene nanomaterials can indeed disrupt bacterial membranes entirely by physical contact. The insertion of graphene sheets into lipid bilayers has also been shown through molecular dynamics simulations by Tu *et al.* to occur spon-

taneously when the lateral edges are oriented towards the cell membrane, allowing penetration and subsequent stabilization of the sp^2 domains with the hydrophobic inner region of the bilayer.[73]

The exposure of these lateral edges to bacterial membranes has even been found to cause movement of phospholipids along the membrane resulting in extraction of lipids.[26,73] According to the results by Perreault[32] and Liu,[26] the antibacterial activity of graphene nanosheets appears to be dependent on their size. It was concluded in both studies that increasing graphene sheet sizes afford higher antibacterial activity *via* disruption of bacterial cell membranes in suspension. This was also recognized experimentally by Liu *et al.* who systematically decreased the size of GO sheets by increasing post-synthetic sonication duration.[26] Sonication treatment for 0 to 240 min produced GO sheets with sizes ranging from 0.753 to 0.01 μm^2 and an average thickness of 1 nm which corresponded to roughly one monolayer of GO. Cell viability was measured by exposing the GO sheets (40 $\mu g\ mL^{-1}$) to an *E. coli* suspension (106–107 CFU mL^{-1}) for 2 h while shaking at 250 rpm and using a colony-counting method with serial dilutions. The viability of bacterial cells was severely diminished in the presence of larger GO sheets in comparison to smaller sizes (Fig. 11A), with the largest GO sheets decreasing viability by 97.7%, in stark contrast to the smallest GO sheets which only decreased the viability by 5.5%. As larger GO sheets have an increased number of sites for oxygen adsorption, the difference in antibacterial activity could be due to oxidative stress. The oxidative stress capacity of the prepared GO sheets were, however, shown *via* Ellman's assay[30] to be independent of GO size, as summarized in Fig. 11B, leading to the conclusion that the primary mechanism of action is membrane damage. This was further supported by AFM images of *E. coli* incubated with the largest (Fig. 11C) and smallest (Fig. 11D) GO sheets of the series for 2 h, which revealed that bacterial cells became completely wrapped by the larger GO sheets and were only adhered by smaller GO sheets. This leads to the conclusion that bacterial inactivation can be achieved by larger GO sheets *via* isolation of affected cells from their environment, which has the consequence of preventing nutrient acquisition and subsequently cellular growth and proliferation. GO sheets have thereby been verified to exert their antibacterial action by a variety of physical means, providing a marked advantage in combating antibiotic-resistant strains of bacteria.

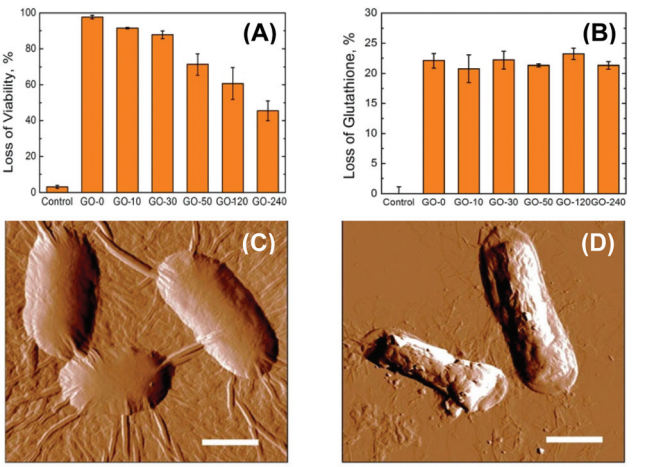

Fig. 11 (A) The viability of *E. coli* cells (5 mL of 10^6–10^7 CFU mL^{-1}) after incubating with GO suspensions (5 mL of 80 $\mu g\ mL^{-1}$) for 2 h with 250 rpm shaking speed at 37 °C. Loss of viability was calculated by the following formula: loss of viability % = (counts of control − counts of samples after incubation with suspensions)/counts of control. (B) Oxidation of glutathione by GO sheets with various lateral sizes. Loss of glutathione (0.4 mM) after *in vitro* incubation with 40 $\mu g\ mL^{-1}$ of GO suspensions for 2 h. The bicarbonate buffer (50 mM at pH = 8.6) without GO was used as a control. AFM images illustrating the effects of (C) large and (D) small GO sheets interacting with *E. coli* cells. The scale bars are 1 μm. Reprinted with permission from ref. 26. Copyright (2012) American Chemical Society.

This has indeed been manifested in a recent study where the interaction of a GO-coated AFM cantilever tip with *E. coli* proved to be repulsive upon exposure to the lipid membrane.[52] The AFM probe was functionalized with 2 g L^{-1} of dopamine at a pH of 8.5, which polymerized on the probe surface under this alkaline condition. The cantilever was then immersed in a GO solution (500 $\mu g\ mL^{-1}$) and placed in close proximity to the cell. The force was recorded as a function of the piezo position while the cantilever approaching the cell was inserted, then withdrawn from the cell membrane. Such repulsive interactions have also been observed by Castrillon *et al.* where an AFM cantilever tip functionalized with GO was utilized to determine the force generated upon approach and removal of the GO tip from the surface of an *E. coli* cell.[52] Their results suggest that the adhesion of GO onto the surface of the bacterial membrane is repulsive in nature. These studies demonstrate the ability of graphene nanostructures to damage bacterial membranes, the degree of which depends on size and composition.

Metal oxide nanostructures have also demonstrated membrane disruption of bacterial cells, as have their GO composite structures. For instance, Zhang *et al.* demonstrated the membrane damaging effects of ZnO nanostructures towards bacterial cells.[74] In their study, the antibacterial activity of 5 commercial ZnO nanostructures was evaluated *via* observations of bacterial growth over time in the presence of varying concentrations of ZnO nanostructures. As seen in Fig. 12, *E. coli* cells in the presence of these ZnO nanostructures had severely damaged membranes and this was attributed, in part, to direct contact of ZnO structures with bacterial cells. This direct damage to cell membranes was also observed for ZnO/GO composite nanostructures by Wang *et al.* in which the growth of bacteria was delayed upon the exposure to ZnO/GO even at <500 $\mu g\ mL^{-1}$.[58] In this case however, the antibacterial activity was found to stem from the released Zn^{2+} ions where the concentration increased over the initial two hours in a culture medium, and saturated at 0.9 $\mu g\ mL^{-1}$, regardless of the concentration of ZnO/GO utilized. The adsorption of 60 μg Zn^{2+} ions was measured in 10 mL culture medium, and the nanocomposite was found to adsorb 39 μg of zinc ions, which, in

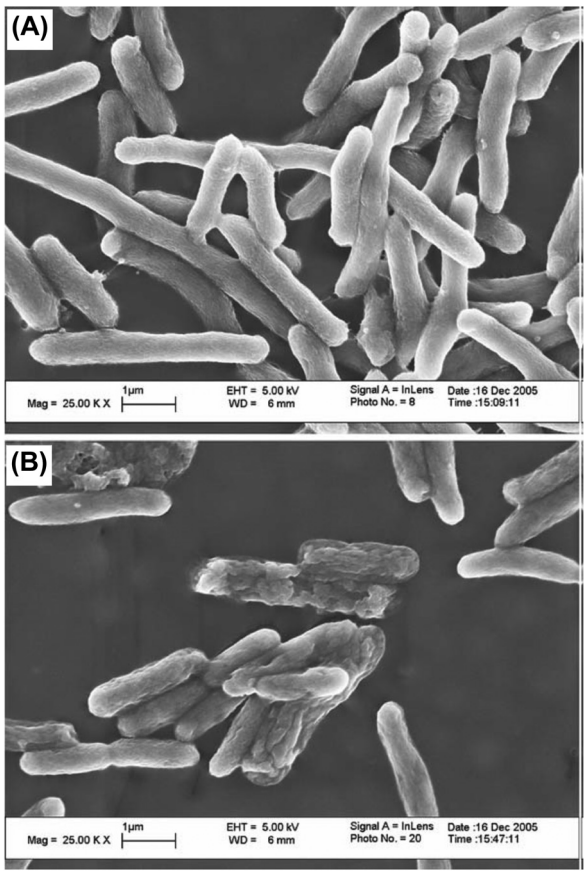

Fig. 12 SEM micrographs of *E. coli* cells (A) before and (B) after treatment with ZnO nanostructures. Reproduced with permission from ref. 74. Copyright (2007) Springer.

conjunction with a change of the zeta potential (ζ) from −11.4 to −9.2 mV, proved that Zn^{2+} ions were adsorbed by GO. This had a significant effect on affected bacterial cells, as seen in SEM images (Fig. 13) where intense pitting and cytoplasmic leakage occurred upon prolonged exposure to these ZnO/GO composites. These results indicate an enhanced antibacterial activity due to the joint effects of ZnO nanostructures and GO sheets, as GO sheets provide more intimate contact with bacterial cells that affords a greatly increased local concentration of Zn^{2+} ions around the cellular membrane. This synergistic effect is analogous to that exhibited by metal nanoparticle–GO composite structures as shown in Fig. 11B, and is representative of the primary advantage of utilizing GO composite structures to enhance a cytotoxic nanomaterial's antibacterial activity. Overall, graphene derivatives are extremely promising as substrates for bactericidal nanomaterials and serve to enhance the cytotoxic effects of the compositing material through enhancement of their activity, but also by providing additional mechanisms of cytotoxicity specific to their graphitic structure.

2.3 Protein dysfunction and transcriptional arrest

Although not typically suggested to be the primary mechanism of action, induced protein dysfunction and transcriptional arrest contribute, sometimes significantly, to the cytotoxicity of graphene nanomaterials. A study by Santhosh *et al.* demonstrated through SDS-PAGE (Fig. 14) that graphene–Fe_3O_4 composite nanostructures (G–Fe_3O_4) cause significantly more protein degradation than Fe_3O_4 alone.[25] This is seen clearly as

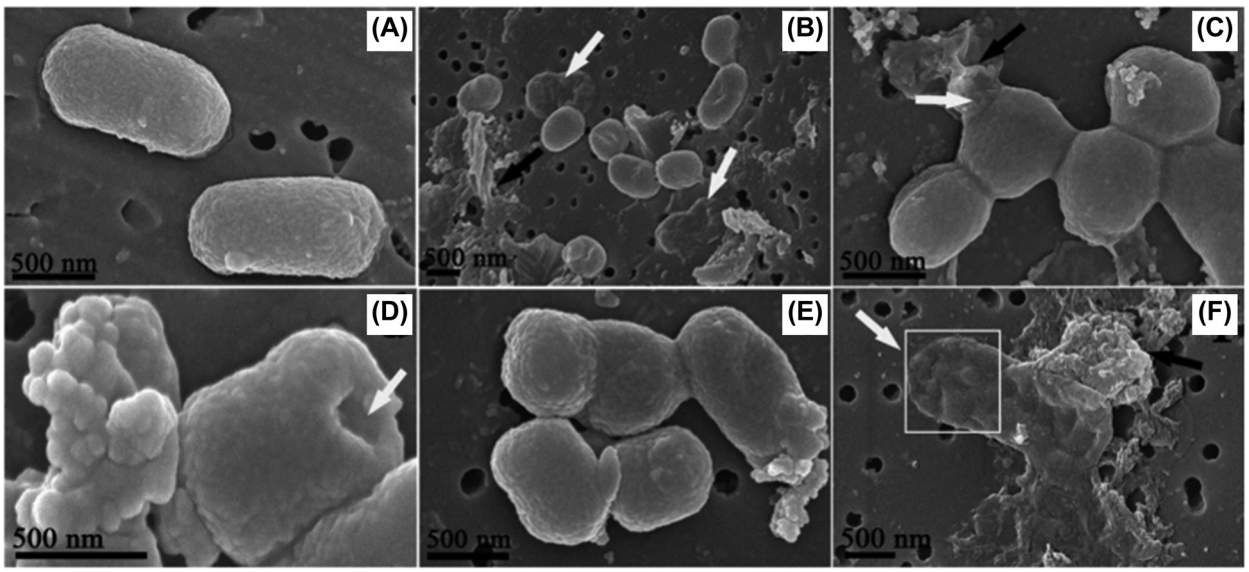

Fig. 13 SEM images of *E. coli*: (A) control; (B–D) *E. coli* treated with ZnO/GO-1 for 24 h; (E and F) *E. coli* treated with ZnO/GO-2 for 24 h. White arrows: broken *E. coli*. Black arrows: the ZnO/GO composites. White square: cytoplasm leakage. Reproduced with permission from ref. 58. Copyright (2014) American Chemical Society.

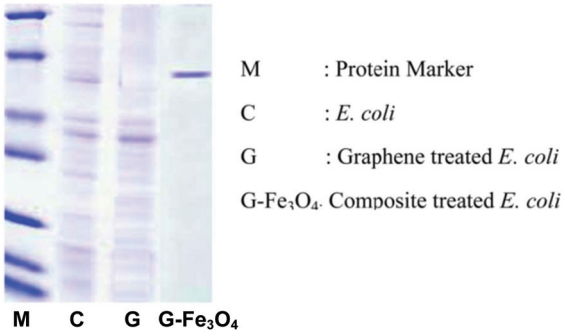

Fig. 14 Photograph of SDS-PAGE gel demonstrating protein degradation induced by graphene (G) and graphene–Fe_3O_4 (G–Fe_3O_4) nanostructures. Reproduced with permission from ref. 25. Copyright (2014) The Royal Society of Chemistry.

lanes having *E. coli* cells treated with G–Fe_3O_4 display only a single band, whereas graphene and *E. coli* cells alone demonstrate multiple bands indicating that G–Fe_3O_4 nanostructures cause the aggregation of cellular proteins. This was attributed to disulfide formation through thiol oxidation catalyzed by the G-Fe_3O_4 composite structure which was quantified *via* Ellman's assay. Akhavan *et al.* also demonstrated through SDS-PAGE, that photocatalytic protein degradation is considerably enhanced in graphene–tungsten oxide composite structures when compared with WO_3 nanoparticles alone.[24] These studies provide direct evidence that protein dysfunction is a significant mechanism of cytotoxicity that can be augmented by graphene composite structures beyond that of the individual components alone.

The interaction of graphene nanostructures with DNA has been observed by several groups, and seemed to occur by π–π stacking interactions.[28,29,75,76] Ren *et al.* demonstrated that DNA–GO interactions relieve supercoiling, while inducing nicks and linearized DNA formation.[28] In the presence of Cu^{2+} ions however, DNA molecules became cleaved, the degree of which was dependent on the concentration of GO (Fig. 15A). This was proposed to occur due to the chelation of Cu^{2+} ions to oxygen functional groups on the GO sheets which then allows for efficient delivery of Cu^{2+} ions to DNA molecules. Circular dichroism and ethidium bromide staining demonstrated that GO sheets intercalate between the base pairs of DNA as expected due to π–π stacking interactions, therefore the localization of chelated Cu^{2+} ions to DNA molecules is enhanced by GO sheets. Their proposed mechanism of DNA cleavage due to GO-chelated Cu^{2+} ions is shown in Fig. 15B, and explains how chelated Cu^{2+} ions can interact with the base pairs of DNA, namely the heterocyclic nitrogen groups which are soft bases. These Cu^{2+}–base interactions can then catalyze the hydrolytic cleavage of the phosphodiester backbone, leading to the observed cleavage.[74] This study demonstrates the potential for GO composites to greatly enhance DNA damage and, given the abundance of metal ions in bacterial cells, highlights the significance of this mechanism of cytotoxicity.

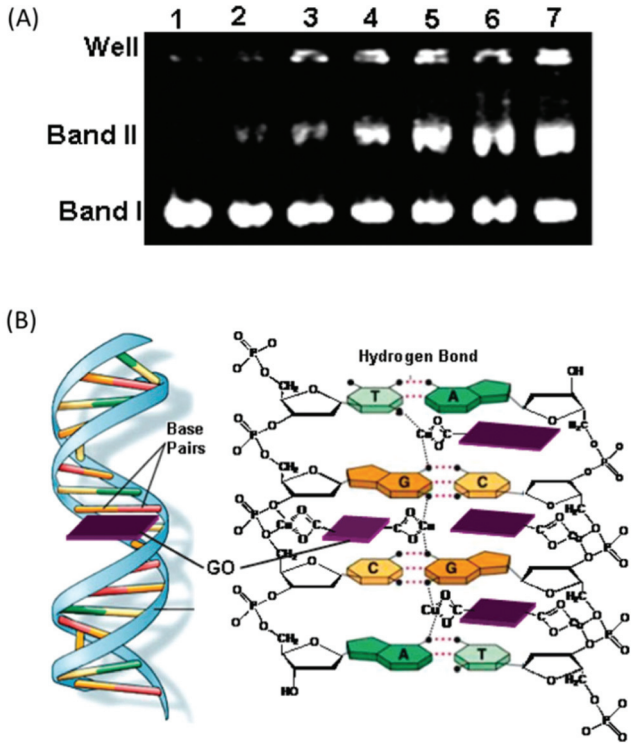

Fig. 15 (A) Photograph of gel electrophoresis experiment demonstrating interactions of DNA with Cu^{2+} ions in the presence of no GO (lane 1), and 12.5 (lane 2), 25 (lane 3), 50 (lane 4), 75 (lane 5), 100 (lane 6), and 125 (lane 7) μg mL^{-1} GO. (B) Proposed mechanism of DNA – graphene oxide – copper ion interactions. Reprinted with permission from ref. 28 Copyright (2010) American Chemical Society.

3. Conclusions and perspectives

The antibacterial activities of graphene-based nanocomposites are promising as a large number of nanostructures have exhibited excellent bactericidal properties and biocompatibility with eukaryotic cells. Although this field is still young, there have already been substantial contributions to the overall understanding of the mechanisms of their activity. There is however, still much to be discovered as the exact molecular and biochemical reactions affording cytotoxicity remains largely unknown. In addition, although graphene derivatives have been shown to enhance the antibacterial activity of metal and metal oxide nanostructures, the exact origins is mostly elusive, likely because there is a considerably complex interplay of interactions between the graphene substrate, the metal or metal–oxide nanoparticle, and the bacterial cell. Future studies should focus on identifying reactions occurring at the surfaces of these composite structures by, for instance, ESR analysis, and more importantly, fluorescence microscopy studies to examine *in vivo* ROS production, thiol oxidation, and membrane damage. In order to gain a deeper understanding of the biochemical mechanisms of action, transcriptomic and proteomic analysis will need to be added to the repertoire of tools used to evaluate nanostructure cytotoxicity. These

experiments will identify the genes and therefore the biomolecular targets of these nanostructures, affording more definitive evaluation of their mechanisms of action. Overall, this extremely interesting application of graphene nanostructures deserves considerable attention from scientists in the fields of both nanomaterials and healthcare in order to realize the next generation of effective antimicrobial materials.

Acknowledgements

This work was supported, in part, by the National Science Foundation (DMR-1409396).

Notes and references

1 H. Y. Mao, S. Laurent, W. Chen, O. Akhavan, M. Imani, A. A. Ashkarran and M. Mahmoudi, *Chem. Rev.*, 2013, **113**, 3407–3424.
2 J. Q. Liu, L. Cui and D. Losic, *Acta Biomater.*, 2013, **9**, 9243–9257.
3 C. McCallion, J. Burthem, K. Rees-Unwin, A. Golovanov and A. Pluen, *Eur. J. Pharm. Biopharm.*, 2016, **104**, 235–250.
4 J. Lee, J. Kim, S. Kim and D. H. Min, *Adv. Drug Delivery Rev.*, 2016, **105**, 275–287.
5 X. L. Ding, H. F. Liu and Y. B. Fan, *Adv. Healthcare Mater.*, 2015, **4**, 1451–1468.
6 S. C. Patel, S. Lee, G. Lalwani, C. Suhrland, S. M. Chowdhury and B. Sitharaman, *Ther. Delivery*, 2016, **7**, 101–116.
7 K. Yang, L. Feng and Z. Liu, *Adv. Drug Delivery Rev.*, 2016, **105**, 228–241.
8 A. Sasidharan, L. S. Panchakarla, A. R. Sadanandan, A. Ashokan, P. Chandran, C. M. Girish, D. Menon, S. V. Nair, C. N. R. Rao and M. Koyakutty, *Small*, 2012, **8**, 1251–1263.
9 Y. B. Zhang, S. F. Ali, E. Dervishi, Y. Xu, Z. R. Li, D. Casciano and A. S. Biris, *ACS Nano*, 2010, **4**, 3181–3186.
10 H. Y. Mao, W. Chen, S. Laurent, C. Thirifays, C. Burtea, F. Rezaee and M. Mahmoudi, *Colloids Surf., B*, 2013, **109**, 212–218.
11 M. C. Duch, G. R. S. Budinger, Y. T. Liang, S. Soberanes, D. Urich, S. E. Chiarella, L. A. Campochiaro, A. Gonzalez, N. S. Chandel, M. C. Hersam and G. M. Mutlu, *Nano Lett.*, 2011, **11**, 5201–5207.
12 S. Barua, S. Thakur, L. Aidew, A. K. Buragohain, P. Chattopadhyay and N. Karak, *RSC Adv.*, 2014, **4**, 9777–9783.
13 M. J. Hajipour, K. M. Fromm, A. A. Ashkarran, D. J. de Aberasturi, I. R. de Larramendi, T. Rojo, V. Serpooshan, W. J. Parak and M. Mahmoudi, *Trends Biotechnol.*, 2012, **30**, 499–511.
14 M. Moritz and M. Geszke-Moritz, *Chem. Eng. J.*, 2013, **228**, 596–613.
15 E. Tegou, M. Magana, A. E. Katsogridaki, A. Ioannidis, V. Raptis, S. Jordan, S. Chatzipanagiotou, S. Chatzandroulis, C. Ornelas and G. P. Tegos, *Biomaterials*, 2016, **89**, 38–55.
16 H. Ji, H. Sun and X. Qu, *Adv. Drug Delivery Rev.*, 2016, **105**, 176–189.
17 L. Shi, J. Chen, L. Teng, L. Wang, G. Zhu, S. Liu, Z. Luo, X. Shi, Y. Wang and L. Ren, *Small*, 2016, **12**, 4165–4184.
18 X. Zou, L. Zhang, Z. Wang and Y. Luo, *J. Am. Chem. Soc.*, 2016, **138**, 2064–2077.
19 H. M. Hegab, A. ElMekawy, L. D. Zou, D. Mulcahy, C. P. Saint and M. Ginic-Markovic, *Carbon*, 2016, **105**, 362–376.
20 S. Szunerits and R. Boukherroub, *J. Mater. Chem. B*, 2016, **4**, 6892–6912.
21 J. H. Li, G. Wang, H. Q. Zhu, M. Zhang, X. H. Zheng, Z. F. Di, X. Y. Liu and X. Wang, *Sci. Rep.*, 2014, **4**, 4359.
22 S. Gurunathan, J. W. Han, A. A. Dayem, V. Eppakayala and J. H. Kim, *Int. J. Nanomed.*, 2012, **7**, 5901–5914.
23 K. Krishnamoorthy, M. Veerapandian, L. H. Zhang, K. Yun and S. J. Kim, *J. Phys. Chem. C*, 2012, **116**, 17280–17287.
24 O. Akhavan, M. Choobtashani and E. Ghaderi, *J. Phys. Chem. C*, 2012, **116**, 9653–9659.
25 C. Santhosh, P. Kollu, S. Doshi, M. Sharma, D. Bahadur, M. T. Vanchinathan, P. Saravanan, B. S. Kim and A. N. Grace, *RSC Adv.*, 2014, **4**, 28300–28308.
26 S. B. Liu, M. Hu, T. H. Zeng, R. Wu, R. R. Jiang, J. Wei, L. Wang, J. Kong and Y. Chen, *Langmuir*, 2012, **28**, 12364–12372.
27 L. Hui, J. G. Piao, J. Auletta, K. Hu, Y. Zhu, T. Meyer, H. Liu and L. Yang, *ACS Appl. Mater. Interfaces*, 2014, **6**, 13183–13190.
28 H. Ren, C. Wang, J. Zhang, X. Zhou, D. Xu, J. Zheng and S. Guo, *ACS Nano*, 2010, **4**, 7169–7174.
29 M. Liu, Q. Zhang, H. Zhao, S. Chen, H. Yu, Y. Zhang and X. Quan, *Chem. Commun.*, 2011, **47**, 4084–4086.
30 G. L. Ellman, K. D. Courtney, V. Andres Jr. and R. M. Feather-Stone, *Biochem. Pharmacol.*, 1961, **7**, 88–95.
31 S. Liu, T. H. Zeng, M. Hofmann, E. Burcombe, J. Wei, R. Jiang, J. Kong and Y. Chen, *ACS Nano*, 2011, **5**, 6971–6980.
32 F. Perreault, A. F. de Faria, S. Nejati and M. Elimelech, *ACS Nano*, 2015, **9**, 7226–7236.
33 A. Ahmad, A. S. Qureshi, L. Li, J. Bao, X. Jia, Y. Xu and X. Guo, *Colloids Surf., B*, 2016, **143**, 490–498.
34 X. Liu, S. Sen, J. Liu, I. Kulaots, D. Geohegan, A. Kane, A. A. Puretzky, C. M. Rouleau, K. L. More, G. T. Palmore and R. H. Hurt, *Small*, 2011, **7**, 2775–2785.
35 M. Zhang, Y. Zhao, L. Yan, R. Peltier, W. Hui, X. Yao, Y. Cui, X. Chen, H. Sun and Z. Wang, *ACS Appl. Mater. Interfaces*, 2016, **8**, 8834–8840.
36 S. S. Nanda, S. S. An and D. K. Yi, *Int. J. Nanomed.*, 2015, **10**, 549–556.
37 S. Gurunathan, J. W. Han, A. A. Dayem, V. Eppakayala and J. H. Kim, *Int. J. Nanomed.*, 2012, **7**, 5901–5914.
38 W. W. He, Y. T. Zhou, W. G. Wamer, M. D. Boudreau and J. J. Yin, *Biomaterials*, 2012, **33**, 7547–7555.

39 G. Applerot, J. Lellouche, A. Lipovsky, Y. Nitzan, R. Lubart, A. Gedanken and E. Banin, *Small*, 2012, **8**, 3326–3337.
40 G. Applerot, A. Lipovsky, R. Dror, N. Perkas, Y. Nitzan, R. Lubart and A. Gedanken, *Adv. Funct. Mater.*, 2009, **19**, 842–852.
41 M. Auffan, W. Achouak, J. Rose, M. A. Roncato, C. Chaneac, D. T. Waite, A. Masion, J. C. Woicik, M. R. Wiesner and J. Y. Bottero, *Environ. Sci. Technol.*, 2008, **42**, 6730–6735.
42 J. Y. Kim, H. J. Park, C. Lee, K. L. Nelson, D. L. Sedlak and J. Yoon, *Appl. Environ. Microbiol.*, 2010, **76**, 7668–7670.
43 C. C. Winterbourn, *Toxicol. Lett.*, 1995, **82–83**, 969–974.
44 S. Goldstein, D. Meyerstein and G. Czapski, *Free Radicals Biol. Med.*, 1993, **15**, 435–445.
45 J. C. Wilks and J. L. Slonczewski, *J. Bacteriol.*, 2007, **189**, 5601–5607.
46 S. J. Stohs and D. Bagchi, *Free Radicals Biol. Med.*, 1995, **18**, 321–336.
47 Y. Zhao, W. F. Chen, C. F. Yuan, Z. Y. Zhu and L. F. Yan, *Chin. J. Chem. Phys.*, 2012, **25**, 335–338.
48 H. H. Yang and R. L. McCreery, *J. Electrochem. Soc.*, 2000, **147**, 3420–3428.
49 D. Y. Qu, *Carbon*, 2007, **45**, 1296–1301.
50 Y. Q. Jiao, F. Qian, Y. Li, G. M. Wang, C. W. Saltikov and J. A. Gralnick, *Bacteriology*, 2011, **193**, 3662–3665.
51 W. B. Hu, C. Peng, W. J. Luo, M. Lv, X. M. Li, D. Li, Q. Huang and C. H. Fan, *ACS Nano*, 2010, **4**, 4317–4323.
52 S. R. V. Castrillon, F. Perreault, A. F. de Faria and M. Elimelech, *Environ. Sci. Technol. Lett.*, 2015, **2**, 112–117.
53 Y. Zhou, R. Chen, T. He, K. Xu, D. Du, N. Zhao, X. Cheng, J. Yang, H. Shi and Y. Lin, *ACS Appl. Mater. Interfaces*, 2016, **8**, 15067–15075.
54 Y. Ouyang, X. Cai, Q. Shi, L. Liu, D. Wan and S. Tan, *Colloids Surf., B*, 2013, **107**, 107–114.
55 V. Jankauskaite, A. Vitkauskiene, A. Lazauskas, J. Baltrusaitis, I. Prosycevas and M. Andrulevicius, *Int. J. Pharm.*, 2016, **511**, 90–97.
56 O. Akhavan and E. Ghaderi, *J. Phys. Chem. C*, 2009, **113**, 20214–20220.
57 B. C. Cao, S. Cao, P. Y. Dong, J. Gao and J. Wang, *Mater. Lett.*, 2013, **93**, 349–352.
58 Y. W. Wang, A. N. Cao, Y. Jiang, I. Zhang, J. H. Liu, Y. F. Liu and H. F. Wang, *ACS Appl. Mater. Interfaces*, 2014, **6**, 2791–2798.
59 A. Nourmohammadi, R. Rahighi, O. Akhavan and A. Moshfegh, *J. Alloys Compd.*, 2014, **612**, 380–385.
60 P. Gao, K. Ng and D. D. Sun, *J. Hazard. Mater.*, 2013, **262**, 826–835.
61 S. Chella, P. Kollu, E. V. P. R. Komarala, S. Doshi, M. Saranya, S. Felix, R. Ramachandran, P. Saravanan, V. L. Koneru, V. Venugopal, S. K. Jeong and A. N. Grace, *Appl. Surf. Sci.*, 2015, **327**, 27–36.
62 K. H. Roehm, *eLS*, 2001, DOI: 10.1038/npg.els.0001373.
63 N. A. Zubir, C. Yacou, J. Motuzas, X. Zhang, X. S. Zhao and J. C. Diniz da Costa, *Chem. Commun.*, 2015, **51**, 9291–9293.
64 R. Khandanlou, M. B. Ahmad, K. Shameli, E. Saki and K. Kalantari, *Int. J. Mol. Sci.*, 2014, **15**, 18466–18483.
65 Z. Lu, C. Mao, M. Meng, S. Liu, Y. Tian, L. Yu, B. Sun and C. M. Li, *J. Colloid Interface Sci.*, 2014, **435**, 8–14.
66 X. Xu, D. Chen, Z. Yi, M. Jiang, L. Wang, Z. Zhou, X. Fan, Y. Wang and D. Hui, *Langmuir*, 2013, **29**, 5573–5580.
67 T. Kavitha, A. I. Gopalan, K. P. Lee and S. Y. Park, *Carbon*, 2012, **50**, 2994–3000.
68 J. S. Kim, E. Kuk, K. N. Yu, J. H. Kim, S. J. Park, H. J. Lee, S. H. Kim, Y. K. Park, Y. H. Park, C. Y. Hwang, Y. K. Kim, Y. S. Lee, D. H. Jeong and M. H. Cho, *Nanomed.: Nanotechnol., Biol. Med.*, 2007, **3**, 95–101.
69 W. Shao, X. Liu, H. Min, G. Dong, Q. Feng and S. Zuo, *ACS Appl. Mater. Interfaces*, 2015, **7**, 6966–6973.
70 E. K. Wujcik and C. N. Monty, *WIREs Nanomed. Nanobiotechnol.*, 2013, **5**, 233–249.
71 J. N. Chen, H. Peng, X. P. Wang, F. Shao, Z. D. Yuan and H. Y. Han, *Nanoscale*, 2014, **6**, 1879–1889.
72 A. V. Titov, P. Kral and R. Pearson, *ACS Nano*, 2010, **4**, 229–234.
73 Y. S. Tu, M. Lv, P. Xiu, T. Huynh, M. Zhang, M. Castelli, Z. R. Liu, Q. Huang, C. H. Fan, H. P. Fang and R. H. Zhou, *Nat. Nanotechnol.*, 2013, **8**, 594–601.
74 L. L. Zhang, Y. H. Jiang, Y. L. Ding, M. Povey and D. York, *J. Nanopart. Res.*, 2007, **9**, 479–489.
75 F. Ortmann, W. G. Schmidt and F. Bechstedt, *Phys. Rev. Lett.*, 2005, **95**, 186101.
76 M. Liu, H. M. Zhao, S. Chen, H. T. Yu and X. Quan, *Chem. Commun.*, 2012, **48**, 564–566.

